

Cite this: *Phys. Chem. Chem. Phys.*, 2011, **13**, 3831–3838

www.rsc.org/pccp

PAPER

## Excitation volumetric effects (EVE) in metal-enhanced fluorescence

A. I. Dragan<sup>a</sup> and C. D. Geddes<sup>\*b</sup>

Received 30th September 2010, Accepted 7th December 2010

DOI: 10.1039/c0cp01986k

Metal-Enhanced Fluorescence (MEF) effects from different density silver island films (SiFs) and the effects of far-field excitation irradiance on the observed enhancement of fluorescence were studied. It is shown that MEF non-linearly depends on silver nanoparticle (NP) size/density, reaching a maximum value for SiFs made at a deposition time (DT) of  $\sim 5$  minutes, *i.e.* just before SiFs become continuous. Numerical simulations of the silver-islands growing on glass revealed that the near-field magnitude depends non-linearly on size and interparticle distance exhibiting dramatic enhancement at  $\sim 10$  nm distance between the NPs. In addition, a remarkable effect of modulation in MEF efficiency by far-field excitation irradiance has been observed, which can be correlated well with numerical simulations that show an excitation power volume dependence. The near-field volume changes non-linearly with far-field power. This unique observation has profound implications in MEF, which has rapidly emerged as a powerful tool in the biosciences and ultimately allows for tunable fluorescence enhancement factors.

### 1. Introduction

Fluorescence based approaches have extensive utilization in the biological sciences, in particular, for the detection of different biological macromolecules (*e.g.* nucleic acids and proteins) and for analysis of their structural dynamics and interactions.<sup>1–5</sup> Successful application of fluorescence-based approaches depends on fluorophore brightness, photostability and an optical response on the registered event (binding, unfolding, dynamics, *etc.*). In many cases it is difficult to select chromophores with these characteristics, especially for a broad range of fluorescence applications. This constraint significantly limits the practical use of fluorescence in bio-medical research and assays. However, discovery of the Metal-Enhanced Fluorescence (MEF) phenomenon, which dramatically enhances the brightness of chromophores several orders of magnitude and, at the same time, increases their photostability, has remarkably improved and broadened fluorescence-based applications in the biosciences.<sup>6–10</sup>

The Metal-Enhanced Fluorescence term was introduced, almost decade ago, by Geddes and Lakowicz,<sup>7</sup> which describes the unique influence of the near-field of a metal-nanoparticle (NP) on the emission properties of chromophores, *i.e.* emission enhancement in the coupled chromophore/NP system. While the exact mechanism of MEF is still under

debate, the approach itself is well established, the effect is due to coupling of a chromophore with surface plasmons in a metal nanoparticle, *i.e.* resonance interaction between electronic systems of a chromophore and nanoparticle.<sup>6,11</sup> Progress in understanding of MEF has been stimulated by numerous experimental studies.<sup>12–17</sup> It has been shown that different metal nanoparticles afford for different MEF properties and enhance fluorescence in plasmon-specific wavelength regions. For example, silver and gold NPs provide for MEF in the visible-NIR region,<sup>18–20</sup> but indium<sup>21</sup>—in the UV region. Recently, we have shown that fluorescence enhancement correlates well with the scattering component of NPs extinction spectra, *i.e.* the magnitude of MEF shows notable wavelength dependence.<sup>22</sup> The change in a NP's size and density also influences the extinction spectrum and, in particular, on its scattering component, which is thought to underpin the MEF enhancement.<sup>11,22</sup> Depending on the conditions and time of silver deposition, the nanoparticles change their shape,<sup>23</sup> the size changes from 10–30 nm to  $> 300$  nm and also changes the inter-particle distance.<sup>24,25</sup>

Another notable experimental observation is that the magnitude of the MEF effect correlates well with the intensity of the near-field generated around NPs in response to incident light irradiance and both parameters decay exponentially with distance from a NP. The near-field around NPs has a specific volume, *i.e.* spatial distribution of high-frequency energy that interacts with the oscillating electronic system of proximal chromophores. This interaction is thought to play an important role in absolute enhancement factor values.

Subsequently, in this study we have investigated the role of silver-islands (nanoparticles that grow on a glass slide upon the wet deposition of silver) size and their density on

<sup>a</sup> Institute of Fluorescence, University of Maryland Baltimore County, 701 East Pratt Street, Baltimore, MD 21202, USA

<sup>b</sup> Institute of Fluorescence and Department of Chemistry and Biochemistry, University of Maryland Baltimore County, 701 East Pratt Street, Baltimore, MD 21202, USA.  
E-mail: geddes@umbc.edu; Fax: +1 410-576-5722;  
Tel: +1 410-576-5723

metal-enhanced fluorescence properties. Also, we have both theoretically and experimentally explored the influence of the far-field irradiance power on near-field intensity, excitation volume and its outcomes on MEF. For the first time we report an approach to tuning MEF enhancement factors, further broadening the potential of this platform technology.

## 2. Experimental section

### 2.1 Materials

Fluorescein, IR-780 perchlorate and whole human blood were purchased from Sigma. Silver nitrate (99.9%), sodium hydroxide (99.996%), ammonium hydroxide (30%) and premium quality silane-prep glass slides (75 × 25 mm) were obtained from Sigma. All chemicals were used as received.

### 2.2 Preparation of silver island films (SiFs)

SiFs were prepared by wet deposition of silver on glass slides according to ref. 13. The deposition time changed from 1 to 7 min. Detailed physical characterization of the SiFs fabricated using this method was recently published.<sup>24</sup>

### 2.3 Preparation of sandwich format samples

A solution of 100 μl of fluorescein (0.5 mM) in TE buffer, pH 7.6 or IR-780 in whole human blood was sandwiched in-between glass and SiF slides (Fig. 1). The IR-780/blood sample was prepared by mixing stock solution of the IR-780 dye in 10% (v/v) ethanol with the whole human blood at ratio 1 : 10 (v/v). Samples were prepared by sandwiching the fluorophore solution in-between Glass slides (G/G) which was used as a control sample. The thickness of the chromophore solution, *i.e.* optical path length, between flush slides was about 1 μm.<sup>24</sup>

### 2.4 Fluorescence measurements

Fluorescence spectra of the samples were collected after mounting the samples on a stand at 90° to the plane of the slide and at 45°, relative to the excitation beam. Recording of the emission spectra was performed with a model HD 2000 Ocean Optics spectrometer (Dunedin, FL). Fluorescein and IR-780 emission were excited by 473 and 785 nm laser lines, respectively. 473 nm (fluorescein) and 785 nm (IR-780)

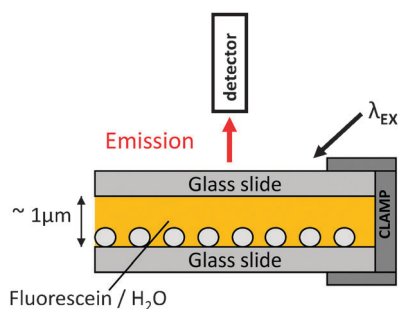


**Fig. 1** SiFs experimental geometry. Fluorescence of fluorescein and IR-780 dye were excited by 473 and 785 nm laser lines, respectively. Emission was collected by the optical fiber and the spectra were measured with a model HD 2000 Ocean Optics spectrometer.

notch filters were used to suppress scattered incident light. Attenuation of the laser power was undertaken using absorptive neutral density filters (Edmunds optics).

### 2.5 Excited state lifetime measurements

Fluorescence decay curves of IR-780 in TE buffer, 10% ethanol, pH 7.6 were measured using a Time Resolved TemPro Fluorescence Lifetime System (Horiba Jobin Yvon, USA). Fluorescence was excited using a 687 nm laser line. The time resolution of the excited state lifetime measurements is less than 20 ps. A 700 nm long-pass filter was used to exclude the excitation light.

### 2.6 FDTD numerical simulations

The 2D FDTD simulations were used for several purposes: to determine the dependence of the near-field intensity around silver nanoparticles (NPs) and their extinction cross-section upon intensity of incident light; to simulate the effect of nanoparticles growing during wet deposition of silver on glass slides and to calculate the dependence of the E-field intensity in between NPs upon inter-particle distance.

In the simulations the incident field is defined as a plane wave with a wave-vector that is normal to the injection surface and the scattered and total fields are monitored during the simulation. Using Lumerical FDTD Solution software, the simulation region was set to 600 × 600 nm<sup>2</sup> with high mesh accuracy. To minimize simulation times and maximize the resolution of field enhancement around the metal particles, a mesh override region was set to 0.1 nm. The overall simulation time was set to 100 fs; calculations were undertaken over the wavelength range 300 to 600 nm.

## 3. Results and discussion

### 3.1 Dependence of metal-enhanced fluorescence (MEF) effect upon the size and density of silver nanoparticles

We have analyzed the influence of silver nanoparticle size and density on the MEF effect for the well-known chromophore, fluorescein. It is known that during the wet deposition process, silver nanoparticles (islands), which grow on a glass surface, increase their size and density depending on the deposition time (DT).<sup>24</sup> At a deposition time DT < 4 min, the size and density of NPs exponentially increases but their surface morphology suggests separate, non-contacting islands on glass. At a DT of 4–5 min silver-island films (SiFs) become quite dense, exhibiting a short, <20 nm, interparticle distance. Silver films become continuous at DT > 6 min. Detailed physical characterization of SiFs produced by our wet deposition technique, including analysis of silver NP size and density, was described in detail in our recent publication.<sup>24</sup>

Fig. 2 shows the effect of SiF deposition time on fluorescence intensity of fluorescein measured for different incident laser powers. Fluorescence intensity values at zero deposition time correspond to fluorescein emission measured for solution placed between glass slides (control sample). The observed changes in fluorescence emission are non-linear: at short DT (1–3 min) the emission intensity increases steeply followed

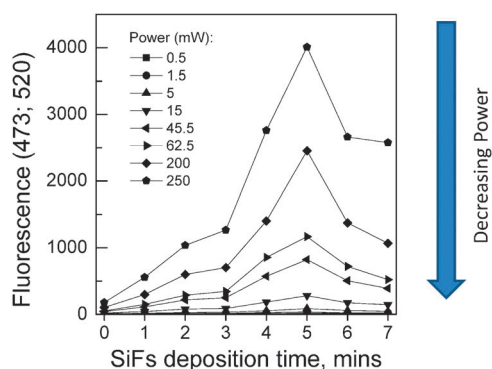


**Fig. 2** Fluorescence intensity of fluorescein as a function of SiF deposition time (from 1 to 7 minutes), obtained with different incident light powers. Fluorescence excitation was at 473 nm and registration of emission at 520 nm.

by a sharp enhancement at a DT of 4–5 minutes and then is reduced at DT = 6–7 min. It is notable that the shape of the observed changes in fluorescence is the same for different powers of laser excitation (Fig. 2), which will be described in detail later in this manuscript.

In general, the observed changes in fluorescence follow the evolution in physical properties of the SiFs, *i.e.* the change in size and density of silver nanoparticles on slides: (1) larger particles more effectively enhance fluorescence of the chromophore; (2) at high silver islands density, when the mean distance between nanoparticles becomes extremely short and electrical conductivity increases, MEF reaches a maximum value; (3) in the condition where particles merge into a continuous metal film, MEF decreases.

One question of importance from Fig. 2 is why this function has a sharp maximum? Certainly, it could not be explained by

the gradual change in SiF landscape. A SiF's landscape does not show any extremum in a course of islands growing on a glass surface. Therefore, we hypothesize that the observed maximum could be caused by the specific change in power volume of the near-field generated around silver-particles by the far-field incident light. The possible reason for such significant increase of the field intensity could be plasmon resonance interparticle interaction that occurs at a certain short distance between silver-islands. This explanation could also explain the sharp drop off in the MEF enhancement, at DT > 5 minutes, by the transformation of NPs into a continuous metal surface.

We have subsequently used FDTD simulations to understand the trends in MEF. For this purpose we have used the following model (Fig. 3), based on the mechanism of silver-islands growing *via* wet chemical deposition. Two nanoparticles, modeled by circles in the 2D-simulation, were positioned at a distance of 60 nm, between their centers; propagation of a far-field is in a plane of the two particles, perpendicular to the axes, connecting their centers; the diameter of the particles increases step-by-step and, consequently, the distance between particles surface shortens. For each step, the FDTD calculations were performed (see Materials and methods). The results of the FDTD calculations clearly demonstrate significant interparticle E-field enhancement which reaches a maximum at a distance of about  $R = 10$  nm, between particles surfaces, and drops down at shorter distances (Fig. 3, bottom-left). An intensive near-field effect at a short, about 10 nm, distance (see spatial distribution of the E-field intensity in X–Y plane at  $R = 10$  nm in Fig. 3, bottom-right) certainly indicates the nature of the non-linear behavior of MEF for different DT SiFs, which strongly supports our hypothesis.

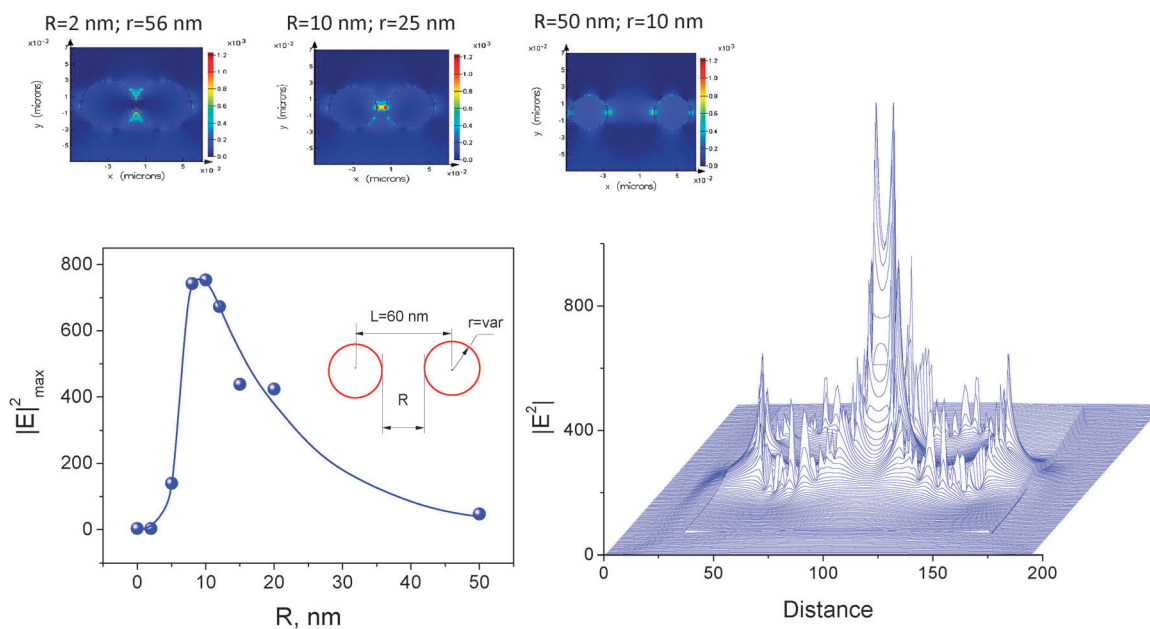


**Fig. 3** (top) Distribution of the E-field (calculated by FDTD simulations) around and between silver nanoparticles that approximate the particle growth on glass slides. (bottom, left) Dependence of E-field intensity maximum between silver particles upon the distance between particles outer surfaces (blue balls). Solid curve is a smooth representation of the change in near-field intensity upon the distance between two particles surfaces. (Inset): Particle geometry parameters used in FDTD calculations. (bottom, right) E-field distribution at  $R = 10$  nm distance between NP surfaces.

### 3.2 Dependence of metal-enhanced fluorescence (MEF) effect upon intensity of incident light

The most remarkable observation made in this study is that the MEF efficiency depends on the intensity of the incident light. Fig. 4 shows the dependence of the fluorescence enhancement factor, *i.e.* the ratio of chromophore emission intensity measured on SiF (glass/SiF sandwich geometry) to the intensity measured from glass (a control glass/glass sample), upon laser power. At low laser power (about 2 mW) the fluorescence enhancement factor (EF) is about 2–4 fold and increases non-linearly with an increase in excitation power, becoming saturated at laser powers >50 mW. For all DTs the character of the function, EF *versus* intensity of excitation, remains the same. The largest EF,  $\approx 25$ , was for SiFs made at DT = 5 min. It should be noted that the EF asymptotic value depends on SiF DT, *i.e.* silver particle size and density (Fig. 4). Therefore, while the main factor which determines the EF “asymptotic” value depends on the property of the SiFs surface (deposition time), the character of the EF *versus* laser power function is clearly underpinned by quite complex photophysical processes that occur between the fluorophore and nanoparticle as a function of laser power excitation.

The magnitude of the MEF effect is thought to be a consequence of the close interaction (coupling) of a chromophore with the near-field, which incident light generates around silver nanoparticles. We performed a series of 2D FDTD simulations with the aim of studying the properties of the near-field and its expansion upon increasing far-field intensity. As can be seen in Fig. 5, an increase in incident far-field intensity ( $|E(\lambda_{\text{ex}})|^2$ ) expands the E-field around the nanoparticle. The calculated maximum intensity of the generated field,  $|E(\lambda_{\text{ex}})_{\text{max}}|^2$ , linearly depends on the intensity of excitation light, *i.e.*  $|E_{\text{max}}|^2 = \beta \times I_{\text{ex}}$ , where  $\beta$  is a slope of the function that does not depend on intensity of excitation (Fig. 6, top), but, as we have shown (see Fig. 3), depends on the size and density of silver islands and dielectric properties of the surrounded NP medium (increase of the refractive index from 1.00 to 1.33 almost twice decreases the slope,

*i.e.*  $\beta = 14$  for vacuum and  $\beta = 7$  for water, Fig. 6). The results of our FDTD calculations also clearly show that the extinction cross-section of the silver NP does not depend on intensity of the excitation (Fig. 6, bottom), where constant values of the absorption and scattering components were observed.

Another interesting result of the FDTD simulations is that the exponential character of the E-field intensity,  $|E|^2$ , changes upon the distance from the NP surface (Fig. 7). It is notable that the decay functions of  $|E|^2$  *vs.* distance ( $D$ ) calculated for silver and gold NPs are the same, which reflects the general character of the near-field energy dissipation. Fitting the data by using the exponential equation:  $|E(D)|^2 = |E(0)|_{\text{max}}^2 e^{-(\alpha D)}$ , where  $|E|_{\text{max}}^2 = \beta \times I_{\text{ex}}$  (for water  $\beta = 7$ ) is a maximum value of the near-field intensity at  $D = 0$  nm,  $I_{\text{ex}}$  is an intensity of excitation (in our case  $|E(0)|_{\text{max}}^2 = 1$ ),  $D$  is a distance from NP and  $\alpha$  is a fitting parameter, revealing  $\alpha = 1/7$ . Therefore the E-field decay function can be written as

$$|E(D)|^2 = |E(0)|_{\text{max}}^2 * e^{-7D} = 7 \times I_{\text{ex}} * e^{-7D} \quad (1)$$

The data obtained using FDTD simulations were applied to the analysis of the near-field spatial distribution. Fig. 8 shows a series of plots exhibiting the change in E-field intensity upon the distance from the NP surface calculated for different intensities of incident light using eqn (1). It can be seen that spatial propagation of the near-field is a non-linear function of excitation energy (*i.e.* laser power), which has a tendency of decaying with distance. Fig. 8, center, shows how the laser power dependent function of the E-field (for this example the magnitude of the field was constant,  $|E|^2 = 0.5$  a.u.) spreads along the axis normal to the NP surface.

To understand volumetric properties of the E-field generated around the NP by the far-field we applied a simple model to the studied system: we determined the E-field volume (magnitude  $|E|^2 = \text{const}$ ) as a volume of a sphere minus the NP volume:

$$V = 4/3\pi((D + R)^3 - R^3), \quad (2)$$

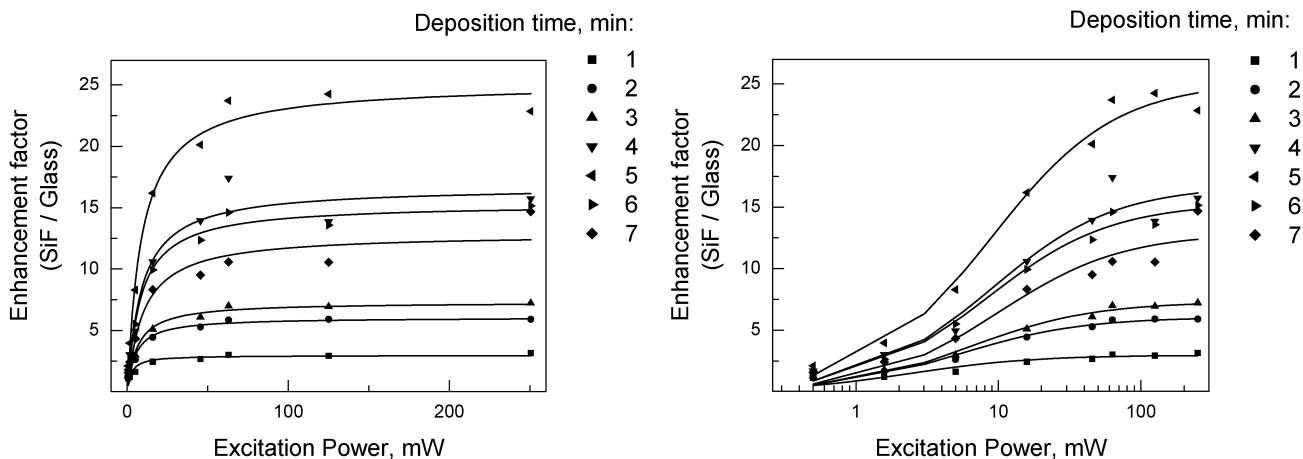


**Fig. 4** (left) The dependence of enhancement factor of fluorescein upon laser excitation power for SiFs fabricated at deposition times ranging from 1 to 7 minutes. (right) The same data plotted with a  $\log_{10}$  laser power axis. Enhancement factor is defined as the ratio of fluorescence intensity on SiFs (glass/SiF sandwich) to the fluorescence observed from a glass control (glass/glass sandwich).

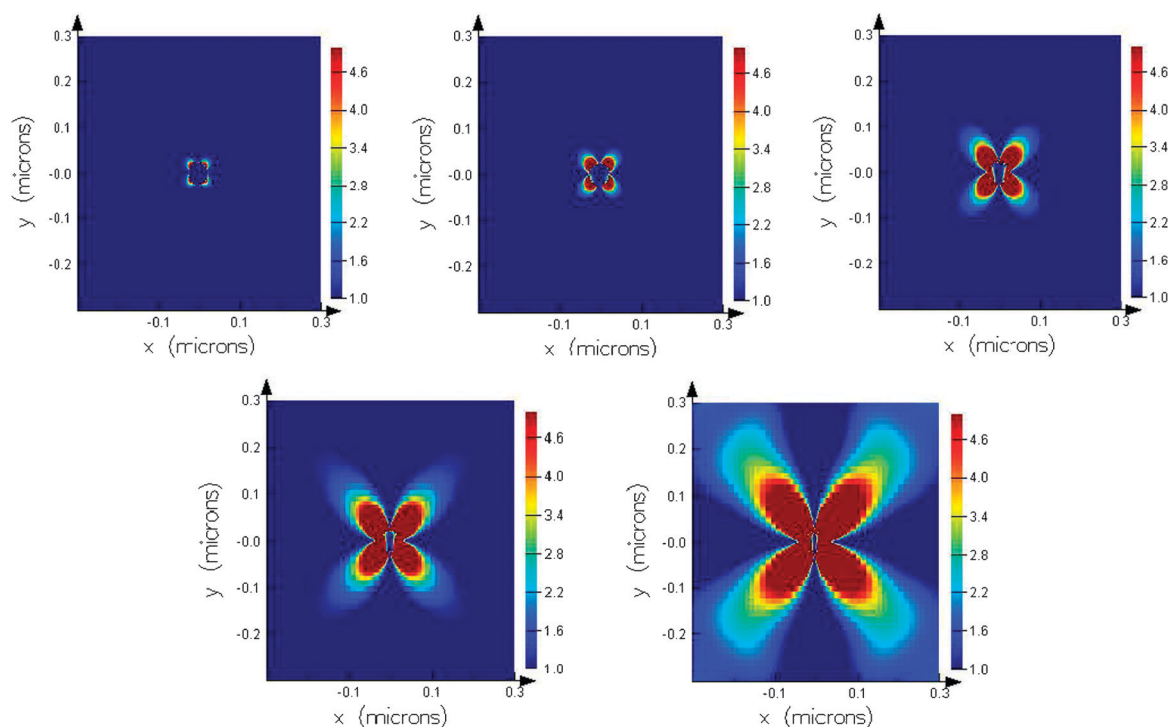


**Fig. 5** Distribution of near-field intensity around a 50 nm Ag-NP upon intensity of incident light. From left to right and from top to bottom:  $I_{\text{ex}} = 1, 16, 36, 64, 100$  a.u.; near-field intensity is between  $|E|_{\text{min}}^2 = 1$  and  $|E|_{\text{max}}^2 = 5$ ; wavelength 345 nm.

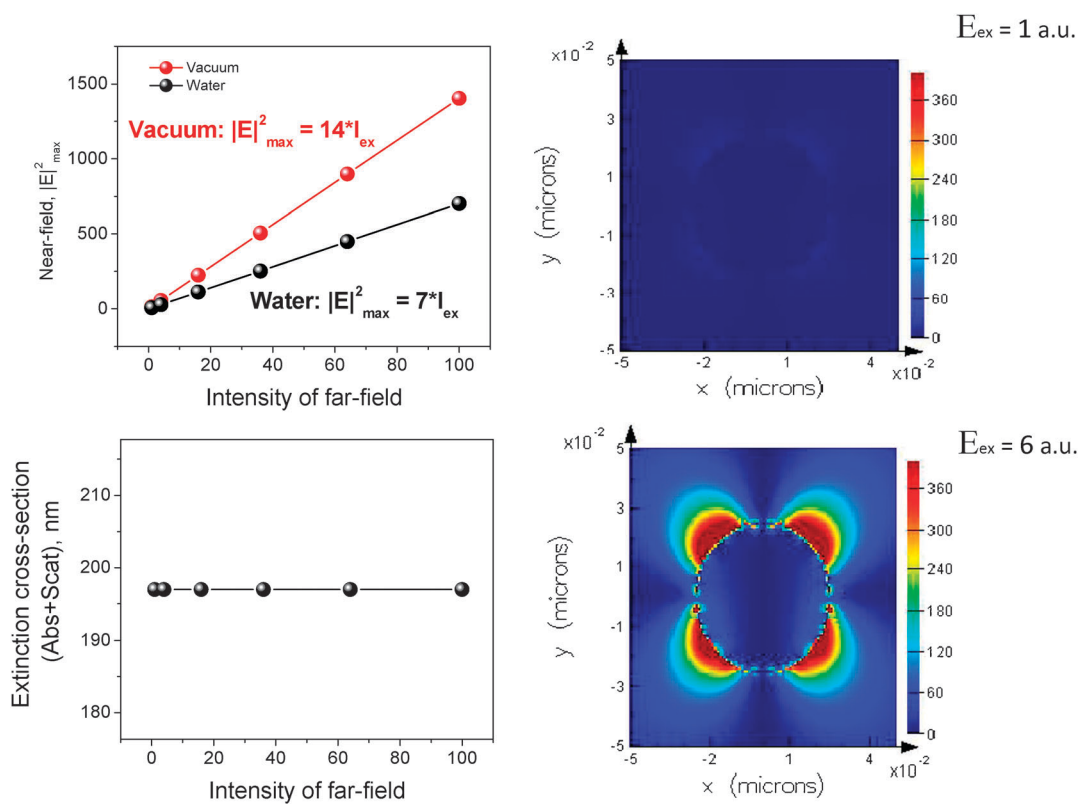


**Fig. 6** (top, left) Intensity of the near-field linearly depends on far-field excitation intensity. (bottom, left) Cross-section of 50 nm Ag nanoparticle does not depend on intensity of incident light. (right) Images of near-field distribution around Ag-nanoparticle at two different amplitudes of the far-field,  $E_{\text{ex}} = 1$  and 6 a.u.

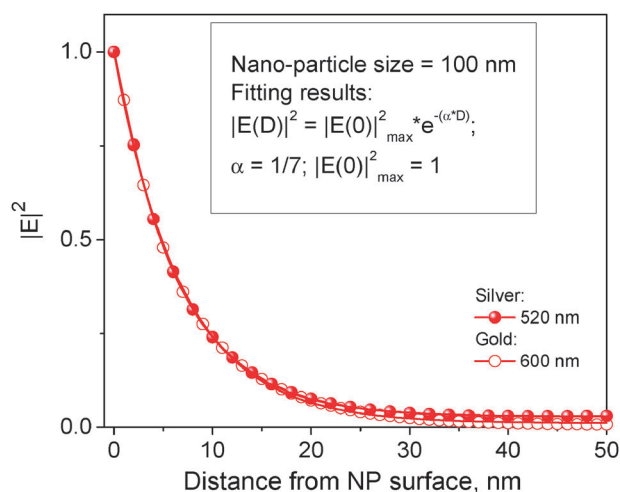


**Fig. 7** Normalized intensity of the near-field depends exponentially upon the distance from the metal (silver, gold) nanoparticle surface. The 2D FDTD calculations were undertaken for 100 nm Ag and Au nanoparticles (NPs) and obtained data were fitted using an exponential function (inset).

where  $R = 50$  nm is a NP radius and  $D$  is a distance of near-field ( $|E|^2 = \text{constant}$ ) from the NP:

$$D = \ln(7 \times I_{\text{ex}}/(|E|^2))/\alpha, \quad (3)$$

where  $|E|^2 = \text{constant} = 0.5$ ,  $\alpha = 1/7$ .

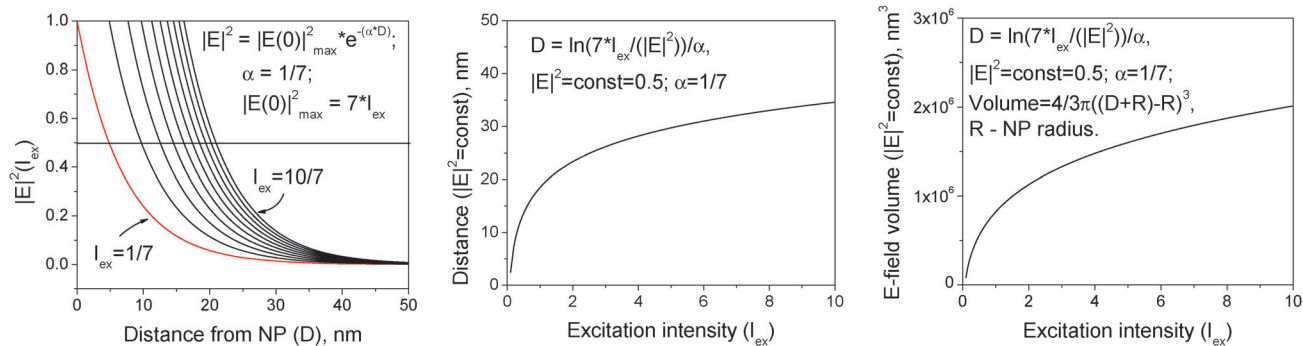


**Fig. 8** (left) Near-field decay functions plotted for different intensities of incident light. (center) Expansion of E-field along the distance from the NP surface upon intensity of excitation; (right) Near-field volume dependence upon intensity of excitation, *i.e.* EVE.

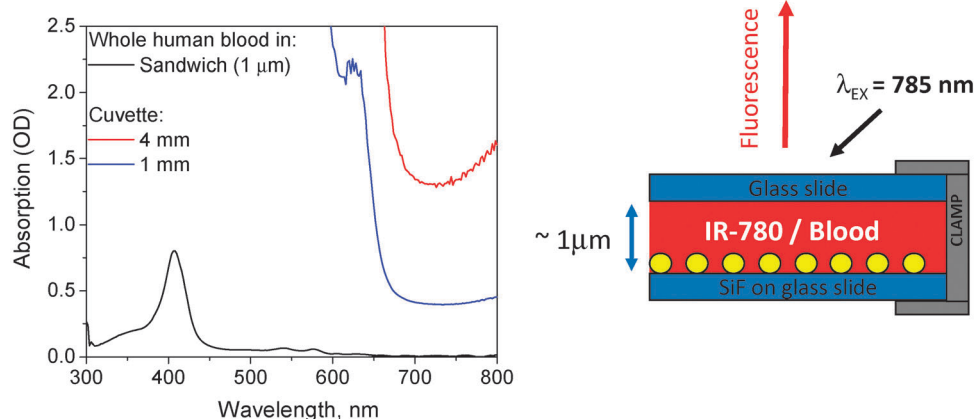


**Fig. 9** (left) Absorption spectra of a human whole blood sample in-between glass slides, 'sandwich geometry', (sample thickness is about 1  $\mu\text{m}$ ); in 4 mm and 1 mm cuvettes. Blood absorption minimum is in the range of 700–800 nm. (right) Experimental setup for the measurement of the near-infra-red (NIR)-MEF for IR-780 dye in whole human blood.

Plotted in Fig. 8 (right) function (2) shows similar non-linear character of change, *i.e.* non-linear character of the E-field volume propagation (E-field volumetric effect) *versus* the energy of the incident light.

Subsequently in this work, we propose that the E-field volumetric effect calculated using FDTD simulations explains the observed changes in metal-enhanced fluorescence (MEF) shown in Fig. 4 as a function of excitation laser power. This result has significant important practical applications in MEF, in the simplest sense, the ability to modulate MEF as a function of excitation power. To the best of our knowledge this is the first report of excitation effects in the Metal-Enhanced Fluorescence literature.<sup>6</sup>

### 3.3 Application of MEF excitation volumetric effect (MEF-EVE) to whole blood-based assays

Biological assays based on the measurement of fluorescence of a chromophore label in whole blood have certain limitations underpinned by the strong optical absorption of blood samples,<sup>26</sup> which invariably decreases a dye's fluorescence signal. To subsequently improve the fluorescence approach in analysis of blood samples, containing typical a NIR-dye, we have investigated the use of both near-field volume and laser power irradiance to improve fluorophore detection.

Typical absorption spectra of whole blood are shown in Fig. 9 (left). Blood has a relatively high transparency

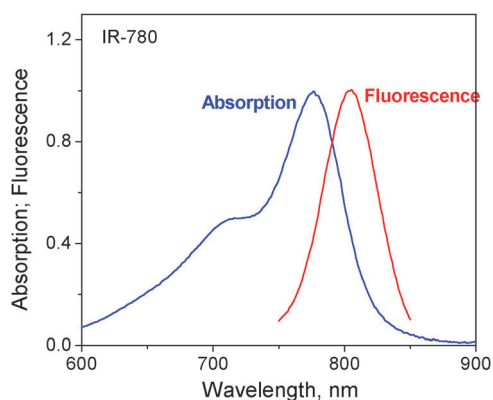


**Fig. 10** Absorption and fluorescence spectra of IR-780 in 10% ethanol. Spectra are normalized. Position of absorption maximum is 776 nm and fluorescence is at 804 nm. Fluorescence decay of IR-780 is single-exponential:  $\tau = 0.42$  ns;  $\chi^2 = 1.5$ .

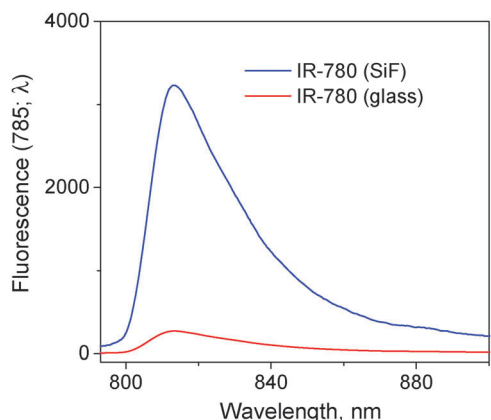


**Fig. 11** Fluorescence spectra of IR-780 measured using an Ocean optics fluorometer on SiFs and on glass slides. Excitation was using a 785 nm laser line; a 785 nm notch filter was used to cut off the excitation in the emission channel. Dye was dissolved in 10% ethanol. SiF slides were prepared using 5 min silver deposition time.

“window” in the range of wavelengths from 700 to 800 nm, which can be used in fluorescence-based assays. It should be noted that the overall absorption could be significantly

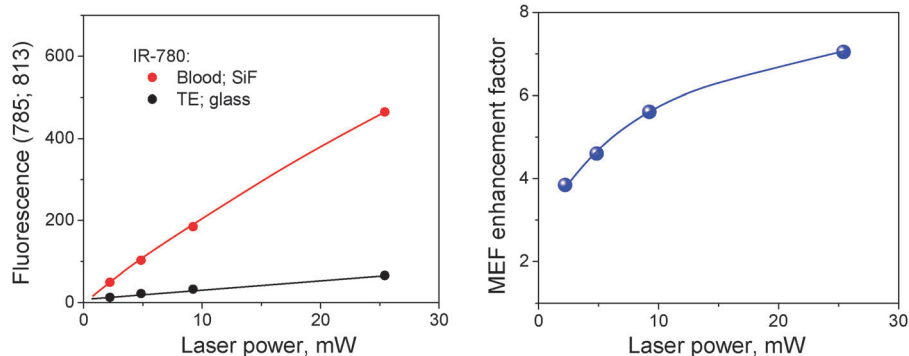


**Fig. 12** (left) Dependence of IR-780 fluorescence upon 785 nm-laser power on SiF (whole human blood in between glass/SiF slides) and on glass (buffer in between glass/glass slides). Concentration of IR-780 in both samples was identical. (right) Dependence of the metal-enhanced fluorescence (MEF) effect upon laser power. Original laser power is 70 mW. Absorptive neutral density filters were used to change the incident laser power from 25 to 2 mW. SiF slides were prepared using 5 min silver deposition time.

decreased by placing the blood sample in between two glass slides. In this case the thickness of the sample, optical path length, is about 1  $\mu\text{m}$  (see Fig. 9 (left)), *i.e.* optical density decreases about 1000-fold.

To study MEF effects in blood we have used a “sandwich” geometry of our samples, Fig. 9 (right), and the near-infra-red (NIR) dye, IR-780, which absorbs and emits light in the blood transparency “window”, Fig. 10, sometimes also referred to as the optical therapeutic window. Fluorescence of IR-780 is weak and characterized by a short excited state lifetime of 0.42 ns. Fluorescence spectra of IR-780 solution placed in-between glass/glass slides, excited using a 785 nm laser line (a 785 nm notch filter was used to cut off excitation in a registration channel), are shown in Fig. 11. The brightness of the IR-780 solution significantly,  $\sim 12$ -fold, increases in the presence of silver nanoparticles (SiFs), *i.e.* when solution is in-between glass and SiF slides (see Fig. 9 (right)), *i.e.* metal amplified.

The changes in fluorescence emission of IR-780/Blood on silver films and on glass are shown in Fig. 12 (left). Fig. 12 (right) shows that the MEF effect, *i.e.* a ratio of the fluorescence intensity on silver to the intensity on glass, increases upon an increased intensity of the incident far-field excitation light. The obtained result clearly demonstrates that the overall enhancement of fluorescence (MEF) depends on far-field energy, further supporting an E-field volumetric effect (EVE). The practical meaning of the results is the significant enhancement in fluorescence-based assays due to MEF-EVE in assays utilizing whole blood samples and the tuning of MEF and thus overall fluorescence brightness.

## 4. Conclusions

MEF non-linearly depends on silver nanoparticle (NP) size and density reaching a maximum value for SiFs made at a deposition time (DT) of 5 minutes, *i.e.* just before the SiF becomes continuous. The FDTD simulations revealed that the near-field intensity depends on size and interparticle distance showing a dramatic enhancement at  $\sim 10$  nm distance in between the NPs. This enhancement of near-field intensity as a result of interparticle plasmon resonance interaction explains the changes in MEF observed experimentally.

A remarkable effect of the modulation of MEF efficiency by far-field excitation power has been observed. FDTD simulations have revealed a link between the MEF effect and the E-field volume, a hitherto unreported E-field volume effect in MEF, EVE. Subsequently, the results not only pace the way for a better understanding of MEF, but allow one to tune absolute fluorescence values from a solution of chromophores.

## Abbreviations

MEF	Metal-Enhanced Fluorescence
FDTD	Finite-Difference Time-Domain based numerical simulations
EVE	Excitation Volume Effect
SiFs	Silver Island Films
DT	Deposition Time
NP	Nanoparticle

## Acknowledgements

We thank the University of Maryland Baltimore County and the Institute of Fluorescence for support. The authors thank also the NIH NIBIB for financial support, 5-U54-EB007958-04, 5-U54-EB007949, 5-U54-EB007959, 5-U54-EB007954.

## References

- 1 C. Blum and V. Subramaniam, Single-molecule spectroscopy of fluorescent proteins, *Anal. Bioanal. Chem.*, 2009, **393**(2), 527–541.
- 2 X. Fang, Y. Mi, J. J. Li, T. Beck, S. Schuster and W. Tan, Molecular beacons: fluorogenic probes for living cell study, *Cell Biochem. Biophys.*, 2002, **37**(2), 71–81.
- 3 J. R. Lakowicz, *Principles of fluorescence spectroscopy*, Springer Science + Business Media, LLC, New York, 3rd edn, 2006.
- 4 S. H. Leuba, S. P. Anand, J. M. Harp and S. A. Khan, Expedient placement of two fluorescent dyes for investigating dynamic DNA protein interactions in real time, *Chromosome Res.*, 2008, **16**(3), 451–467.
- 5 T. Terai and T. Nagano, Fluorescent probes for bioimaging applications, *Curr. Opin. Chem. Biol.*, 2008, **12**(5), 515–521.
- 6 *Metal-Enhanced Fluorescence*, ed. Chris D. Geddes, John Wiley & sons, Inc., Hoboken, New Jersey, 2010.
- 7 C. D. Geddes and J. R. Lakowicz, Metal-enhanced fluorescence, *J. Fluoresc.*, 2002, **12**(2), 121–129.
- 8 E. G. Matveeva, I. Gryczynski, A. Barnett, Z. Leonenko, J. R. Lakowicz and Z. Gryczynski, Metal particle-enhanced fluorescent immunoassays on metal mirrors, *Anal. Biochem.*, 2007, **363**(2), 239–245.
- 9 R. Nooney, A. Clifford, X. LeGuevel, O. Stranik, C. McDonagh and B. D. MacCraith, Enhancing the analytical performance of immunoassays that employ metal-enhanced fluorescence, *Anal. Bioanal. Chem.*, 2010, **396**(3), 1127–1134.
- 10 M. Staiano, E. G. Matveeva, M. Rossi, R. Crescenzo, Z. Gryczynski, I. Gryczynski, L. Iozzino, I. Akopova and S. D'Auria, Nanostructured silver-based surfaces: new emergent methodologies for an easy detection of analytes, *ACS Appl. Mater. Interfaces*, 2009, **1**(12), 2909–2916.
- 11 K. Aslan and C. D. Geddes, *Metal-enhanced fluorescence: Progress towards a unified plasmon-fluorophore description*, in *Metal-Enhanced Fluorescence*, ed. C. D. Geddes, John Wiley & Sons, Inc., Hoboken, NJ, 2010, pp. 1–24.
- 12 Y. Chen, K. Munechika and D. S. Ginger, Dependence of fluorescence intensity on the spectral overlap between fluorophores and plasmon resonant single silver nanoparticles, *Nano Lett.*, 2007, **7**, 690–696.
- 13 M. H. Chowdhury, K. Ray, K. Aslan, J. R. Lakowicz and C. D. Geddes, Metal-enhanced fluorescence of phycobiliproteins from heterogeneous plasmonic nanostructures, *J. Phys. Chem. C*, 2007, **111**(51), 18856–18863.
- 14 S. D'Agostino, P. P. Pompa, R. Chiuri, R. J. Phaneuf, D. G. Britti, R. Rinaldi, R. Cingolani and F. Della Sala, Enhanced fluorescence by metal nanospheres on metal substrates, *Opt. Lett.*, 2009, **34**(15), 2381–2383.
- 15 A. I. Dragan, Y. Zhang and C. D. Geddes, Voltage-gated metal-enhanced fluorescence II: Effects of fluorophore concentration on the magnitude of the gated-current, *J. Fluoresc.*, 2009, **19**(2), 369–374.
- 16 S. Mackowski, S. Wormke, A. J. Maier, T. H. Brotsudarmo, H. Harutyunyan, A. Hartschuh, A. O. Govorov, H. Scheer and C. Brauchle, Metal-enhanced fluorescence of chlorophylls in single light-harvesting complexes, *Nano Lett.*, 2008, **8**(2), 558–564.
- 17 Y. Zhang, K. Aslan, M. J. Prevlite and C. D. Geddes, Metal-enhanced e-type fluorescence, *Appl. Phys. Lett.*, 2008, **92**(1), 13905.
- 18 J. P. Anderson, M. Griffiths and V. R. Boveia, Near-infrared fluorescence enhancement using silver island films, *Plasmonics*, 2006, **1**(2–4), 103–110.
- 19 K. Aslan, S. N. Malyn and C. D. Geddes, Metal-enhanced fluorescence from gold surfaces: angular dependent emission, *J. Fluoresc.*, 2007, **17**(1), 7–13.
- 20 A. I. Dragan, E. S. Bishop, J. R. Casas-Finet, R. J. Strouse, M. A. Schenerman and C. D. Geddes, Metal-enhanced PicoGreen fluorescence: application for double-stranded DNA quantification, *Anal. Biochem.*, 2010, **396**(1), 8–12.
- 21 A. I. Dragan and C. D. Geddes, Indium Nanodeposits: A Substrate for Metal-Enhanced Fluorescence in the UV Spectral Region, *J. Appl. Phys.*, 2010, **108**, 094701.
- 22 Y. Zhang, A. Dragan and C. D. Geddes, Wavelength dependence of metal-enhanced fluorescence, *J. Phys. Chem. C*, 2009, **113**(28), 12095–12100.
- 23 K. Aslan, I. Gryczynski, J. Malicka, E. Matveeva, J. R. Lakowicz and C. D. Geddes, Metal-enhanced fluorescence: an emerging tool in biotechnology, *Curr. Opin. Biotechnol.*, 2005, **16**(1), 55–62.
- 24 R. Pribik, A. I. Dragan, Y. Zhang, C. Gaydos and C. D. Geddes, Metal-Enhanced Fluorescence (MEF): Physical characterization of Silver-island films and exploring sample geometries, *Chem. Phys. Lett.*, 2009, **478**(1–3), 70–74.
- 25 L. N. Xu, B. J. Lee, W. L. Hanson and B. Han, Brownian motion induced dynamic near-field interaction between quantum dots and plasmonic nanoparticles in aqueous medium, *Appl. Phys. Lett.*, 2010, **96**, 174101.
- 26 M. Meinke, G. Muller, J. Helfmann and M. Friebel, Empirical model functions to calculate hematocrit-dependent optical properties of human blood, *Appl. Opt.*, 2007, **46**(10), 1742–1753.